Closing the Time-Varying Mass and Heat Budgets for Large Ocean Areas: The Tasman Box

DEAN ROEMMICH, JOHN GILSON, AND JOSH WILLIS

Scripps Institution of Oceanography, University of California, San Diego, La Jolla, California

PHILIP SUTTON

National Institute of Water and Atmospheric Research, Wellington, New Zealand

KEN RIDGWAY

Marine Research, Commonwealth Scientific and Industrial Research Organization, Hobart, Australia

(Manuscript received 23 August 2004, in final form 8 December 2004)

ABSTRACT

The role of oceanic advection in seasonal-to-interannual balances of mass and heat is studied using a 12-yr time series of quarterly eddy-resolving expendable bathythermograph (XBT) surveys around the perimeter of a region the authors call the Tasman Box in the southwestern Pacific. The region contains the South Pacific's subtropical western boundary current system and associated strong mesoscale variability. Mean geostrophic transport in the warm upper ocean (temperature greater than 12°C) is about 3.8 Sv (1 Sv $\equiv 10^6$ $m^3\ s^{-1}$) southward into the box across the Brisbane, Australia–Fiji northern edge. Net outflows are 3.3 Sv eastward across the Auckland, New Zealand–Fiji edge, and 2.7 Sv southward across Sydney, Australia–Wellington, New Zealand. Mean Ekman convergence of 2.2 Sv closes the mass budget. Net water mass conversions in the upper ocean consist of inflow of waters averaging about 26°C and 35.4 psu balanced by outflow at about 18°C and 35.7 psu, and reflect the net evaporation and heat loss in the formation of South Pacific Subtropical Mode Water. The mean heat balance shows good agreement between ocean heat flux convergence (42.3 W m^{-2}), heat loss to the atmosphere from the NCEP–NCAR reanalysis (39.2 W m^{-2}), and heat storage calculated from data in the box interior (1.3 W m^{-2}). On interannual time scales, volume transport through the box ranges from about 1 to 9 Sv, with heat flux convergence ranging from about 20 to 60 W m^{-2}. An interannual balance in the heat budget of the warm layer is achieved to within about 10 W m^{-2} (or 6 W m^{-2} for the upper 100 m alone). Maxima in the advective heat flux convergence occurred in 1993, 1997, and 1999–2000, and corresponded to maxima in air–sea heat loss. The evolution of surface-layer temperature in the region is the residual of nearly equal and opposing effects of ocean heat flux convergence and air–sea exchange. Hence, ocean circulation is a key element in the interannual heat budget of the air–sea climate system in the western boundary current region.

1. Introduction

The subtropical western boundary currents (WBCs) carry large volumes of warm water rapidly from the Tropics to the midlatitude oceans, where there is high evaporation and strong heat loss to the atmosphere. The WBC systems are important elements of the ocean circulation heat engine, removing excess heat from the Tropics and releasing it to the midlatitude atmosphere. Understanding the mean and time-varying characteristics of WBC heat transport is an important challenge for unraveling the heat balance of the coupled climate system.

One such WBC system is that of the East Australian Current (EAC) in the southwestern Pacific (Ridgway and Godfrey 1994; Ridgway and Dunn 2003). The EAC flows southward along the coast of Australia to about 32°S, where the upper layers of the current separate from the coast. Part of the separated flow forms a tight recirculation gyre on the offshore edge of the EAC. The remainder of the upper-layer flow turns east-

Corresponding author address: Dean Roemmich, Scripps Institution of Oceanography, University of California, San Diego, La Jolla, CA 92093-0230.
E-mail: droemmich@ucsd.edu

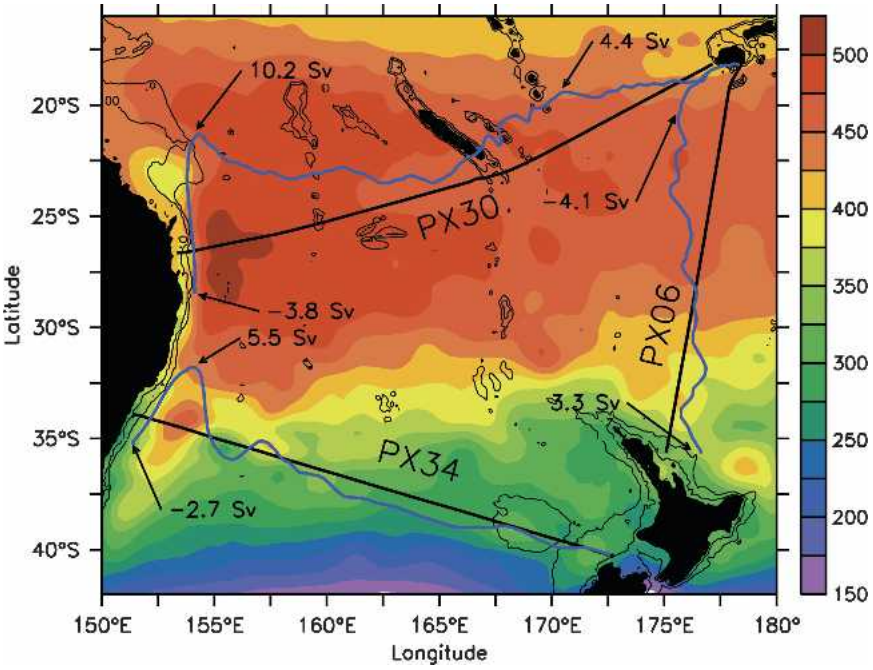

FIG. 1. The mean routes of the Tasman Box HRX transects (black lines) are shown in relation to the mean depth of the 12°C isotherm (background shading). Mean geostrophic transport of waters warmer than 12°C (relative to 2000 m, dark blue), integrated from the Fiji endpoint on PX06 and PX31, or the New Zealand endpoint on PX34, is overlaid. The zero for the integrated transport lines is the HRX track line. Extreme and endpoint integrated transport values (Sv) are included.

ward—with part of the eastward flow reattaching to the northern coast of New Zealand as the East Auckland Current (EAUC; Stanton et al. 1997) and the remainder flowing northeastward in a series of current filaments.

We initiated a long-term observational program in this region in 1986, starting with a quarterly high-resolution expendable bathythermograph (HRX) transect between Auckland, New Zealand, and Fiji (Fig. 1; Roemmich and Cornuelle 1990; Morris et al. 1996). This transect crosses the eastward outflow, including the EAUC and the northeastward filaments of the separated EAC. In 1991, two more quarterly HRX transects were added. One of these crosses the inflowing EAC and its recirculation east of Brisbane, Australia (27°S). The other crosses part of the EAC that overshoots the separation point east of Sydney, Australia (34°S). The three HRX transects (Fig. 1), and the coastlines between them, completely enclose a region of the northern Tasman Sea and the South Fiji Basin that we refer to as the Tasman Box.

There have been previous investigations of the interannual heat budget of the Kuroshio and Gulf Stream systems, summarized by Kelly and Dong (2004). These have pointed to a significant role for ocean advection in the surface-layer heat budget of WBC regions. Lacking adequate subsurface datasets, these studies relied on simple models and on inference from altimetric height to estimate oceanic advection. The present work estimates the role of advection directly from the HRX dataset and extends the earlier studies to a different geographical domain—that of the WBC system of the southwestern Pacific.

A study of mean heat transport in the Tasman region was carried out by Ridgway and Godfrey (1994). A preliminary analysis of interannual heat advection in the Tasman Box (Sprintall et al. 1995) suggested a significant role in regional climate variability based on the first three years of HRX sampling. We expand on the earlier work by exploiting the much longer HRX time series and additional supplementary data now available. Little is known about interannual variability of ocean circulation and transport. Are interannual fluctuations in EAC volume transport stored in the WBC region, or carried eastward into the ocean interior? What are the dominant terms in the interannual heat balance? Does air–sea flux show signals that are also seen in ocean heat transport or storage? Because of their swift and highly variable flows, the WBC systems are regions where ocean transport of heat is likely to

play a strong role in the interannual balance. The goals are to expand our knowledge of WBC systems in general as well as to understand the variability in a part of the southwestern Pacific with strong regional interest.

The present work aims to close the mean and seasonal-to-interannual heat budget in the warm water layer (temperatures greater than 12°C) of the Tasman Box during the period 1991–2002. It includes ocean heat transport estimates from the HRX transects, storage in the interior of the box from broadscale XBT and satellite altimetric height data, and air–sea fluxes from operational and reanalysis products.

2. Data

Although the HRX transects form the primary data for the Tasman Box study, a combination of datasets provides a more comprehensive picture. The additional data include top-to-bottom conductivity–temperature–depth (CTD) surveys made at least once along each leg of the box, satellite altimetric height (AH) for the period from late 1992 to the present, broadscale XBT data in the Tasman Box interior, and air–sea flux products from operational model analyses.

a. HRX transects

The three HRX routes that make up the Tasman Box are shown in Fig. 1: the eastern edge PX06 (Auckland–Fiji), the northern edge PX30 (Brisbane–Fiji), and the southern edge PX34 (Wellington, New Zealand–Sydney). Along each edge, 44 transects have been obtained during 1991–2002, at approximately 3-month intervals. A scientist or technician rides the ship on PX06 and PX30 in order to obtain closely spaced profiles—about 10–20-km separation through the boundary currents to about 50 km in the interior. Most of the PX34 transects have been carried out by the ships' officers, with sampling at slightly reduced spatial resolution. Dates and data for all cruises are displayed on the Internet at http://www-hrx.ucsd.edu. These data are used for estimating the mean and time-varying geostrophic velocity, volume transport, and heat flux convergence across the faces of the Tasman Box.

b. Top-to-bottom CTD transects

Each of the three HRX transects around the Tasman Box has been sampled by a research vessel (R/V) CTD cruise. Transects were made by R/V *Knorr* along PX06 in September 1992 [World Ocean Circulation Experiment (WOCE) cruise P-14C] and by R/V *Franklin* along PX30 in March 1999 and along PX34 in May 2001. These data are combined with other deep data from the World Ocean Dataset 2001 (WOD01) and used to test and adjust the 800-m reference level (for geostrophic calculations), which is the deepest extent of the XBT data.

c. Altimetric height and broadscale thermal data

A merged Topographic Ocean Experiment (TOPEX)/Poseidon and European Remote Sensing (ERS) altimetric sea level product from Archiving, Validation and Interpretation of Satellite Oceanographic Data (AVISO; Ducet et al. 2000) provided the AH data on a 1/3° × 1/3° Mercator grid every 7 days. First, AH was used in combination with broadscale thermal data to estimate heat storage in the interior of the Tasman Box (Willis et al. 2003), as well as to estimate the time-varying depth of the 12°C isotherm in the interior of the box. The southwestern Pacific is relatively well sampled, with about 3000 temperature profiles per year collected in or near the Tasman Box (though these are very inhomogeneous in space). Using the AH/thermal data combination, the large-scale heat storage estimates of Willis et al. (2003) are accurate to about 5 W m^{-2} for a 1-yr mean. An additional use of AH in the present study is to estimate and correct for temporal aliasing by the quarterly sampling scheme of the HRX network, as described below. Finally, AH data are used to estimate the time-varying geostrophic flow at the sea surface for comparison with the time-varying flow relative to 800-m depth from HRX data.

d. Air–sea fluxes

Interannual variability of air–sea heat exchange was examined using the National Centers for Environmental Prediction–National Center for Atmospheric Research (NCEP–NCAR) reanalysis (Kalnay et al. 1996) and European Centre for Medium-Range Weather Forecasts (ECMWF) operational analysis (ECMWF 1993). The primary use of these products here is comparison of air–sea heat exchange with ocean heat storage and heat flux convergence. The ECMWF wind stress was used for calculation of Ekman transport across the HRX lines. Mean surface winds enter the box from the southwest and exit toward the northwest, with mean Ekman transport into the box along all three lines.

3. The mean balance in the warm water layers

The 12-yr (1991–2002) means of temperature, salinity, geostrophic velocity, and steric height along each of the Tasman Box HRX transects are shown in Figs. 2a–c. The mean temperature fields are based on 44 cruises along each side of the box, with near-even distribution

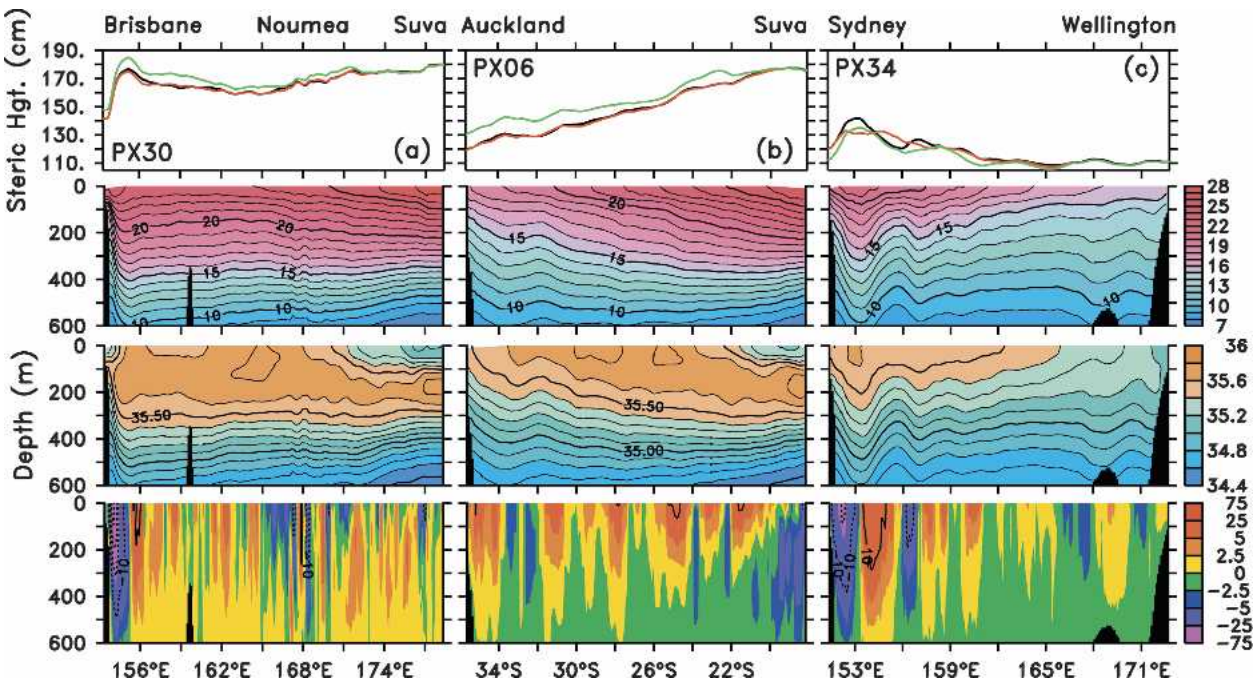

FIG. 2. (top) Mean steric height and (second) temperature, (third) salinity, and (bottom) geostrophic velocity for (a) PX30, (b) PX06, and (c) PX34. Steric height lines are the mean (0–800 m) from all XBT data (black), dealiased using altimetric height (red), and adjusted to 2000-m reference level (green).

by season and year. The salinity fields for each cruise are calculated from the measured temperature and a temperature–salinity (T–S) relation constructed from historical data along each side, with T–S varying along-track.

The steric height and geostrophic velocity were initially calculated using an 800-m reference level, the deepest level consistently sampled by the XBTs. For the mean field, the reference level was adjusted to 2000-m depth using deep shear calculated from the one-time CTD transects, plus additional data from WOD01 close to the HRX tracks. The one-time CTD transects contain small-scale features that may be unrepresentative of the mean, such as boundary current meanders. We therefore applied the reference-level correction as a constant velocity at 800 m for each transect, though results differed little if a spatially varying correction was applied. These correction velocities were 0.74 cm s^{-1} westward across PX06, 0.38 cm s^{-1} northward across PX30, and 0.45 cm s^{-1} southward across PX34. The net inflow of intermediate water across PX06 and outflow across the other two transects is consistent with the one-time CTD transects, historical analyses (Ridgway and Dunn 2003; Reid 1986), and WOCE floats at 1000 m (Davis 1998). The deep reference-level adjustment has substantial impact on the net transports across each side [3–6-Sv (1 Sv $\equiv 10^6$ m^3 s^{-1}) change for each side in the warm water layer, temperatures greater than 12°C]. After the adjustment, a residual of 1.4 Sv out of the box in the net geostrophic plus Ekman transport above 12°C was removed by applying an additional 0.05 cm s^{-1} into the box uniformly around the perimeter. For this mass-balanced system the mean geostrophic transports above 12°C are 3.77 Sv southward across PX30, 3.25 Sv eastward across PX06, and 2.73 Sv southward across PX34, plus Ekman convergence totaling 2.21 Sv.

In addition to the reference-level adjustment, another issue is how accurately the 44-cruise mean approximates the true decadal mean for the Tasman Box. For the 10-yr overlap period of HRX transects with altimetric height, 1993–2002, AH was subsampled along the sides of the box at the times of HRX cruises and compared to the AH mean from the complete AH dataset. The difference between the subsampled and complete AH means is applied as a correction to the steric height in Fig. 2, producing the red lines in the upper panels of the figure from the black ones. It is seen that temporal sampling errors in the 44-cruise mean are not a substantial problem except near Sydney in PX34, where strong 100-day periodicity seen in AH is aliased by the quarterly HRX cruises. The aliasing issue will be considered further in the context of interannual variability. Over the 10-yr period there is a small positive

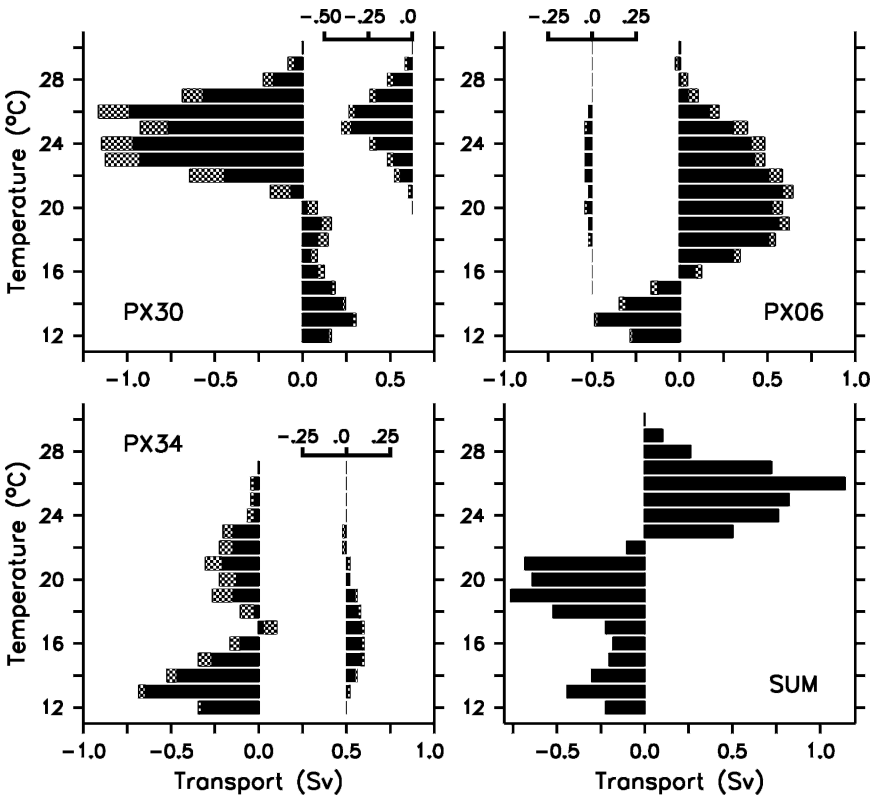

FIG. 3. Mean geostrophic transport (black, main x axis) and Ekman transport (black, inset upper x axis) per unit temperature for waters warmer than 12°C flowing across PX30, PX06, and PX34 individually (positive is northward or eastward), and the sum of transport into the box (positive in). Note that all x axes have the same scale. The standard error is displayed as an extension of each bar (checkered).

trend in AH, consistent with the net heat storage of 1.3 W m^{-2} during that period (Willis et al. 2003).

The mean geostrophic velocity across the three sides of the box, shown in the bottom panels of Fig. 2, is consistent with the regional circulation described by Ridgway and Dunn (2003). In PX30 (Fig. 2a), the EAC flowing southward along the western boundary is seen entering the Tasman Box near Brisbane. There is a tight northward recirculation on the EAC's offshore edge as well as a broader and weaker recirculation. Weak southward flow with high temporal and spatial variability is seen where the ship track passes just south of New Caledonia at about 168°E.

The EAC begins to separate from the coast north of Sydney, with portions of the current continuing southward across PX34 (Fig. 2c) before turning and recrossing the PX34 transect as northward flow. The EAC separation occurs in stages (e.g., Ridgway and Dunn 2003), and the separated EAC flows eastward into the box interior in several filaments. The eastern end of PX34 near Wellington is the most poleward and coldest part of the box and is relatively quiescent.

In PX06 north of Auckland, the EAUC is seen flowing out of the box at the left edge of the bottom panel of Fig. 2b. A broader eastward flow is seen at 27°–32°S, with narrow stronger filaments at 25° and 21°S. All of the eastward filaments appear fairly shallow. However, we have observed the EAUC at 1000–1600-m depth in Argo float trajectories, and a mooring in the EAUC showed mean flow of 3.2 cm s^{-1} toward the southeast at 1500 m (Stanton and Sutton 2003). The shallow penetration of the EAUC in Fig. 2b is an artifact of the smoothed reference velocity. The eastward filaments have high statistical significance. They can be seen in independent multiyear subsets of the 17-yr PX06 time series and are shown in Ridgway and Dunn's (2003) schematic diagram of the regional circulation (their Fig. 7).

As surface waters flow through the Tasman Box, they are modified by air–sea exchanges of heat and freshwater, emerging from the box cooler and saltier on the whole through net heat loss and net evaporation. Figure 3 shows the mean transport across each transect in 1°C temperature classes, as well as the net transport

into or out of the box at each temperature. The inflow of warm waters occurs largely across PX30 in the EAC, at temperatures centered on 24°–26°C. Outflows occur in the eastward filaments crossing PX06 in a broad range of temperatures centered at about 20°C, and southward across PX34 at about 13°C. Contained within the flow leaving the box across PX06 is water with temperature and salinity characteristics that are similar to or slightly warmer than Southwest Pacific Subtropical Mode Water (STMW, 17°C and 35.5 psu; Roemmich and Cornuelle 1992). Approximately two-thirds of the PX06 eastward transport in the 16°–18° range is of water with low vertical temperature gradient, indicative of STMW. The Tasman Box can be thought of as a factory for STMW preconditioning and production through air–sea exchanges.

The focus here is the mean and time-varying mass and heat balance of the upper ocean, and it is necessary to specify a fixed control volume for the heat balance calculations. The temporal mean depth of the 12°C isotherm is chosen as the base of the control volume, with the sides consisting of the mean HRX tracks and adjoining coastlines (Fig. 1). The 12°C isotherm is below the surface mixed layer in winter everywhere in the box, so its depth is not directly modified by air–sea heat exchange. Salinity variations are not great along the 12°C isotherm in the box (Fig. 2), so this surface approximates an isopycnal. The time-varying 12°C isotherm will be treated as a material surface in the interannual balance. That is, its spatially averaged vertical excursions of order 10 m on interannual time scales will be used to estimate the interannual transport variations across the bottom of the control volume. If z_{12} is the depth of the 12°C isotherm and an overbar denotes the time mean, then

$$w_{\bar{z}_{12}} \approx \frac{\partial \bar{z}_{12}}{\partial t}. \quad (1)$$

The mean heat flux convergence due to ocean currents through the control volume during the study period, 1991–2002 is described by the warm-to-cool temperature conversions of Fig. 3. This amounts to 0.140 pW, or 42.3 W m^{-2} averaged over the area of the box. This result was not very sensitive to the reference-level adjustment, being 0.139 pW if the 800-m reference level was used instead of 2000-m depth. The sensitivity of the mean heat flux convergence to other error sources was also investigated. These included sampling errors (in the 44-cruise means) and the assumption that the small mass flux divergence, relative to 2000-m depth, is balanced by uniform inward flow around the box. From these sources, errors in the mean heat flux convergence total less than 5 W m^{-2}. Heat storage in the layer above 12°C over the 10-yr period with AH data was 1.3 W m^{-2} ± 0.5 (Willis et al. 2003). The mean heat loss from the ocean by air–sea fluxes, 1991–2002, was 28.7 W m^{-2} in ECMWF operational surface analyses and 39.2 W m^{-2} in NCEP–NCAR reanalysis data. Combining these estimates (Table 1), the residual of heat flux convergence, air–sea flux, and storage is 12.3 W m^{-2} using ECMWF air–sea fluxes, and 1.8 W m^{-2} using NCEP–NCAR (Table 1).

TABLE 1. Mean heat balance of the Tasman Box (W m^{-2} heat gain by the ocean). The small residual using NCEP–NCAR reanalysis air–sea fluxes indicates that it is most consistent with the time mean heat flux convergence and storage estimates.

1) Heat flux convergence	42.3 ± 5 W m^{-2}
2) Storage	1.3 ± 0.5 W m^{-2}
3) Air–sea flux	ECMWF: −28.7 W m^{-2}
	NCEP: −39.2 W m^{-2}
Residual (1 – 2 + 3)	ECMWF: 12.3 W m^{-2}
	NCEP: 1.8 W m^{-2}

4. Annual variability in geostrophic transport

With 44 cruises along each leg of the Tasman Box, there are only about 4 cruises in a given month and not enough to calculate accurate monthly means. Instead, we linearly interpolated the quarterly cruises to obtain evenly spaced monthly values, and then averaged over all Januarys, etc. (Fig. 4, solid line). Annual variability estimated from a harmonic fit to the (uninterpolated) time series is very similar (Fig. 4, dashed). The southward transport across PX30 and eastward transport across PX06 in the first half of the year are both less than the annual mean by about 1.4 Sv. During the second half of the year they are similarly greater than the annual mean. Hence, the transport through the Tasman Box has a significant, but not a large, annual variability. PX34 annual transport variability appears similar to the other two in magnitude, but with maximum outflow there lagging PX30 inflow by a couple of months.

The annual variability in ocean heat flux convergence—from combining the time-varying geostrophic and Ekman velocity with temperature—is similarly small. XBT-measured 5-m temperature is used to approximate the temperature of the Ekman transport (Wijffels et al. 1994). The amplitude is about 12 W m^{-2}, with maximum heating (54 W m^{-2}) in March. This is much smaller than air–sea flux annual variability, which has amplitude of about 150 W m^{-2} in the ECMWF data and maximum heating (112 W m^{-2}) in December.

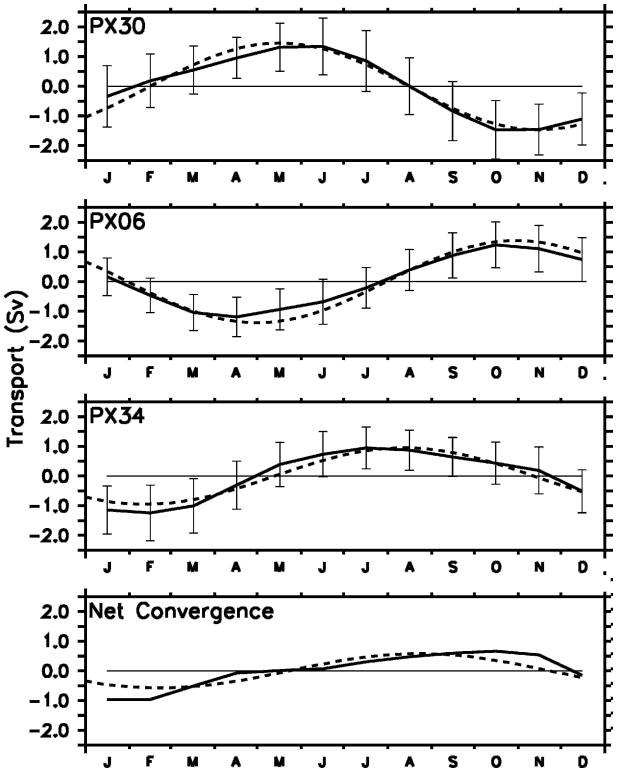

FIG. 4. Monthly means of transport for waters warmer than 12°C across PX30, PX06, and PX34 (positive is northward or eastward) and the sum of transports into the box (positive in). Error bars are the standard error. The annual harmonic, determined from a least squares fit of sine/cosine pairs to each transport time series, is also displayed (dashed).

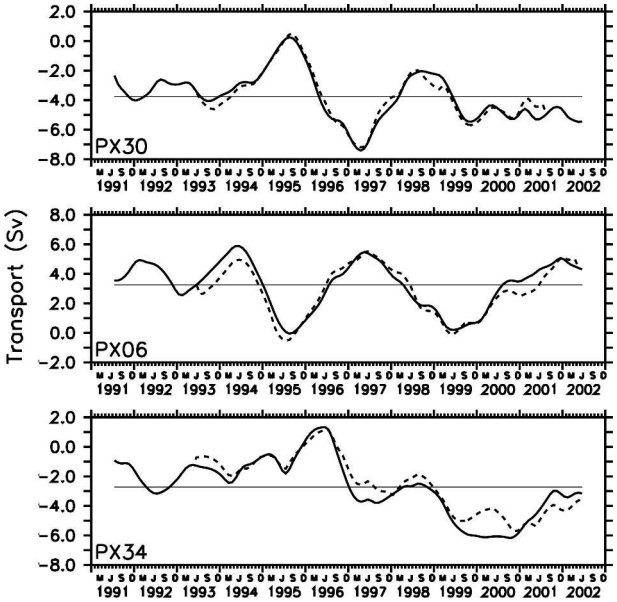

FIG. 5. Interannual (12-month running mean) variability of volume transport (Sv) in waters warmer than 12°C across PX30, PX06, and PX34. The 12-yr means are referenced to 2000 m, the interannual fluctuations to 800 m. "Dealiased" volume transport, using AH, is also shown (dashed lines).

5. Interannual volume transport variability

Figure 5 shows the interannual variability in geostrophic transport of waters warmer than 12°C for each transect. Values are 12-month running means from the interpolated monthly values and are very similar to four-cruise running means. The interannual anomalies are referenced to 800 m because of the lack of deep data. As an alternative, AH sea surface slope anomalies were used to reference the interannual variability in geostrophic transport, and this is discussed in the next section. Also shown is the 12-yr mean, referenced to 2000 m as discussed in section 3.

Covarying transport occurred across the northern (PX30) and eastern (PX06) sides of the box (Fig. 5). The prominent maxima and minima in eastward outflow across PX06 usually coincide with maxima and minima in the southward inflow across PX30. The interannual range in transports relative to 800-m depth is about 6 Sv. Examination of AH data subsampled at HRX cruise dates, compared to the complete AH dataset (Fig. 5), indicates that these interannual signals are not artifacts of temporal aliasing.[1]

Transport estimates across PX34 are at times more problematic than the other lines. The inshore edge of the EAC was poorly sampled by two cruises in mid-1996, with the missing southward flow contributing to spuriously high northward transport estimates at that time. Altimetric height data near Sydney shows strong 100-day variability that is aliased into low frequencies by the quarterly cruises (Figs. 5 and 2). The "dealiasing" correction is as large as 2 Sv in 2000, but overall it appears that the quarterly transects still do a reasonable job of capturing the interannual variability in transport.

It is of interest to distinguish between variability in the transport of waters through the Tasman Box—flow that enters on one side and exits on another—versus variability in transport resulting in accumulation or reduction of warm water in the box interior. These will be referred to as throughflow transport variability and convergent transport variability, respectively. The con-

[1] Transports are estimated from AH data using a simple regression of AH anomaly onto a 0–800-m density anomaly, varying with location around the box (Gilson et al. 1998). Then the difference between the transports estimated in this way using the full AH dataset and AH subsampled at cruise times is calculated. This difference is applied to the solid lines in Fig. 6 to produce the "dealiased" estimate (dashed lines).

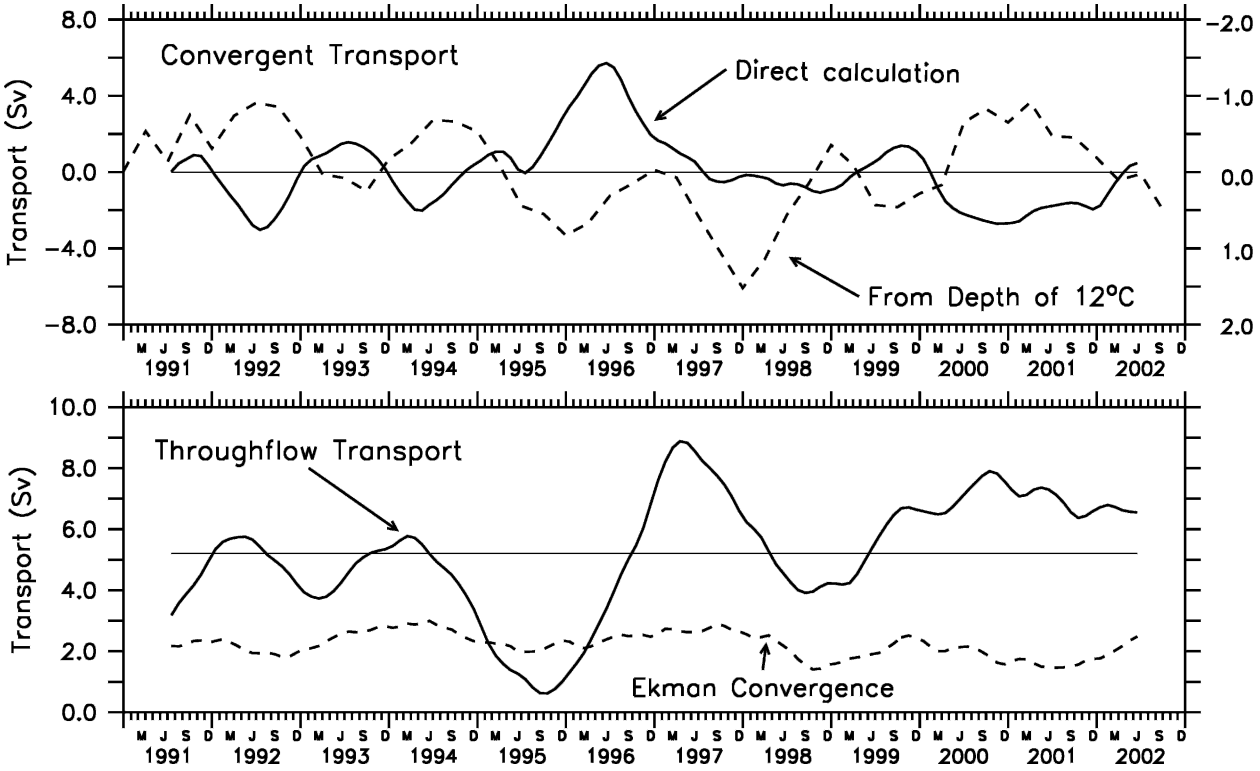

FIG. 6. (a) Convergent transport estimated directly from the sum of transports in Fig. 5 (CT_V, solid line, scale at left) and calculated indirectly from the depth of the 12°C isotherm (CT_12, dashed line, scale at right). Note the reversed and expanded scale at right for the latter calculation. (b) Throughflow transport [Eq. (4), solid line] estimated directly from the transports in Fig. 5, and Ekman convergence (sum across all three sides of the box, dashed).

vergent transport (CT_V) is defined as the sum of volume transports into the region:

$$\text{CT\_}V = V_{34} - V_{30} - V_{06}, \tag{2}$$

where V_{34}, V_{30}, and V_{06} are the volume transports of water warmer than 12°C across the respective lines. Positive indicates northward in the case of V_{34} and V_{30} or eastward for V_{06}. A direct calculation of CT_V, from summing the interannual geostrophic transports' values shown in Fig. 5, and including the corresponding Ekman transports, is shown in Fig. 6. However, the convergent transport is sensitive to the choice of reference level (here 800 m) as well as being subject to the aliasing and other sampling problems noted earlier. Because of the reference-level uncertainty, it is difficult to assign realistic error bounds to the direct CT_V estimate. An independent and more reliable estimate of convergent transport, CT_12, is made by estimating vertical velocity, w, at the base of the box from time variations in the depth of the 12°C isotherm in the box interior (1):

$$\text{CT\_12} = \int_{\text{box}} w_{\bar{z}_{12}}\, dA \approx \int_{\text{box}} \frac{\partial z_{12}}{\partial t}\, dA. \tag{3}$$

A conservative error bound on this calculation, based on estimation of z_{12} from broadscale XBT data and AH (Willis et al. 2003) is 0.4 Sv for interannual variations. In Fig. 6, CT_12 is shown on a reversed and expanded scale from CT_V to emphasize two points. First, it is well correlated with CT_V. The largest discrepancies are in mid-1996 and late 1997/early 1998. We have noted a significant error in PX34 transport during 1996. The cause of the discrepancy during the 1997–98 period is uncertain, but Willis et al. (2003) do note a strong, deep warming feature moving into the Tasman Box region at this time associated with the 1997/98 El Niño. The signal, which extended deeper than 800 m, would induce a time-varying reference velocity, which was not corrected for in CT_V. Second, the amplitude of CT_12 is only about 1/3 of CT_V. This indicates that although the pattern of CT_V is realistic, there is a problem with the reference level. Either a shallower reference level or a deeper one for the time-varying flow will produce a similar time-varying pattern of CT_V, but with diminished amplitude. Equivalently, CT_V can be constrained to be equal to CT_12 by applying a reference velocity at 800 m. In section 6 this time-varying refer-

ence velocity adjustment is made, arbitrarily, in the EAC near Brisbane, where the vertical and time-averaged temperature in waters above 12°C is a maximum for the box (18.28°C). The impact of this transport ambiguity on the heat budget is discussed in the next section.

The throughflow transport (TT) is the amount of warm water entering the box from the north and leaving it toward the east or the south. A primary element of the throughflow transport, and of the heat flux into the box, is the western boundary current system. The EAC enters from the north, is cooled in the box interior, and flows out mostly to the east in the EAUC and other filaments. One cannot unambiguously separate these narrow currents from their recirculating components or from deeper counterflows. Therefore the TT is simply defined as the average of the net inflow transport across the PX30 line and the net outflow across the PX06 and PX34 lines:

$$\mathrm{TT} = (-V_{30} + V_{06} - V_{34})/2. \quad (4)$$

The interannual pattern of TT shown in Fig. 6 has a range of about 8 Sv, from the minimum of 1 Sv in 1995 to 9 Sv in 1997. As with CT_V, it is likely that adjustments to TT from velocity at 800 m are significant. An adjustment to the 800-m velocity field was tried using altimetric height, as discussed below.

Throughflow transport is not synonymous with EAC transport, because TT includes recirculating components and other flow elements integrated over the 2000-km-scale sides of the box. The pattern of TT bears a weak resemblance to that of Ekman convergence (Fig. 6), because the two are related via Sverdrup dynamics. Periods of greater wind stress curl in 1991–92, 1993–94, 1997, and 1999–2000 increase the Ekman convergence. This in turn drives equatorward transport in the ocean interior, which is balanced by poleward flow in the boundary current. The TT includes the entire boundary current flow plus a part of the interior. The absence of an obvious lag suggests that the TT variability is controlled by winds in the western part of the ocean.

Several conclusions are drawn from the patterns of CT_12 and TT in Fig. 6. First, the storage of waters above 12°C in the Tasman Box is much less than the variability in flow through the region on interannual time scales. Correcting TT by the same time-varying adjustment made to CT_V (resulting in CT_12) results in little difference to the interannual character of TT. Second, the differences in the two estimates of CT (CT_V and CT_12) indicate there is a fairly complicated vertical structure to the time-varying transport, and significant shear below the 800-m level sampled by XBTs. Finally, since waters leaving the box are cooler than those entering, the variability in TT is anticipated to have some impact on the interannual heat budget. The pathway of waters passing through the box determines how long they are exposed to atmospheric cooling, and is also important.

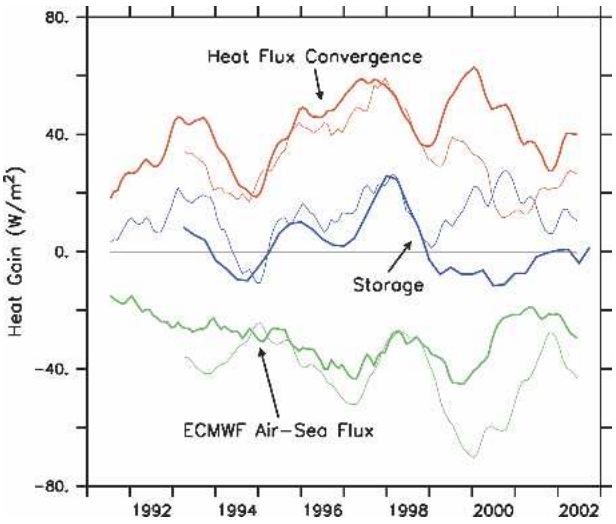

FIG. 7. Interannual heat budget of the Tasman Box for waters warmer than 12°C, expressed as heat gain by the ocean: ocean heat flux convergence (thick red line), storage (thick blue line), and ECMWF air–sea flux (thick green line). The thin lines are estimates of each component as the residual of the other two; i.e., the thin blue line is the estimate of storage from the sum of ocean heat flux convergence and air–sea exchange.

6. The interannual heat budget

a. Heat flux convergence

The interannual variability in Tasman Box heat flux convergence (Fig. 7, thick red line) is estimated by combining the geostrophic (Fig. 5) and Ekman volume transport variability with the temperature field on the three sides of the box. The heat flux convergence is

$$\mathrm{HF} = \int_{\bar{z}_{12}}^{0} \int_{0}^{L} \rho c_p v T \, dz \, dx + \rho c_p (\mathrm{CT}) T_{\bar{z}_{12}}. \quad (5)$$

The heat flux convergence is calculated for the fixed control volume, and the mass balance is closed by the requirement that the net transport across the sides of the box is equal to the transport across the bottom (CT_V = CT_12).

Over the 12-yr period of the study, there are three main peaks in the Tasman Box heat flux convergence (Fig. 7), occurring in 1993, 1996–97, and early 2000. The range in values is about 40 W m^{-2}, from a minimum of about 20 to a maximum of more than 60 W m^{-2}. The broad peak in 1996–97 is due partly to the maximum in

throughflow transport that occurs in 1997, and partly to convergent transport (downward motion of 12°C isotherm) in early 1996 and late 1997. The variability in heat flux convergence is complex, with fluctuations in throughflow transport, surface-layer temperature, and horizontal convergence all playing a role.

The largest error in the estimate of heat flux convergence is that due to ambiguity in the time-varying reference velocity, $v'(800)$. Above it was assumed that $v'(800)$ is zero, except as needed in the EAC so that horizontal convergence balances vertical displacement of the 12°C isotherm. An alternative solution satisfies the convergence constraint by applying a uniform horizontal reference velocity around the perimeter of the box (average temperature above the 12°C isotherm = 17.1°C) instead of in the EAC, and differs by only a few watts per meter squared. Any distribution of $v'(800)$, varying arbitrarily around the box, subject to a constraint of horizontal nondivergence in the warm water layer, could in principle be added to these solutions. Altimetric height is used here to estimate the magnitude of heat flux error due to this ambiguity.

Time-varying reference velocities were estimated from AH (i.e., sea surface slope anomalies) along each transect. First, AH was used to calculate surface geostrophic velocity anomalies $[v'_{\mathrm{AH}}(0)]$, and then the HRX thermal-wind shear between 0 and 800 m $[v'_{\mathrm{XBT}}(0) - v'_{\mathrm{XBT}}(800)]$ was subtracted to estimate $v'_{\mathrm{AH}}(800)$:

$$v'_{\mathrm{AH}}(800) = v'_{\mathrm{AH}}(0) - [v'_{\mathrm{XBT}}(0) - v'_{\mathrm{XBT}}(800)]. \quad (6)$$

However, while estimates of $v'_{\mathrm{AH}}(0)$ have good signal-to-noise ratio, the same is not true for the much smaller $v'_{\mathrm{AH}}(800)$. For each transect, the spatial mean of $v'_{\mathrm{AH}}(800)$ had rms values of about 0.3 cm s^{-1} corresponding to height differences between the transect endpoints of about 4 cm. This is close to the error in estimating AH endpoint differences (the AH estimates degrade near land boundaries). The transport estimates derived using AH had some unrealistic features, such as increasing the imbalance in horizontal convergence above the 12°C isotherm, even when the AH values were smoothed interannually to reduce noise. It is concluded that, in this case, the AH adjustment does not improve the initial calculation with $v'_{\mathrm{XBT}}(800)$ equal to zero. However, the difference between the calculation using AH and the original calculation with $v'_{\mathrm{XBT}}(800)$ equal to zero serves as a realistic error bound. When both solutions were constrained to have the horizontal convergence equal to that implied by z_{12}, the rms difference in heat flux convergence between the two solutions was 9 W m^{-2}.

A second, smaller error is due to errors in the mass flux convergence, as estimated from z_{12}. For the latter, errors in isotherm depth (Willis et al. 2003) are equivalent to 0.4 Sv rms of convergence. For water entering the box via the EAC, with a vertically averaged temperature of 18.3°C, and balanced by flow downward through the bottom of the box at 12°C, 0.4 Sv of transport error is equivalent to 3 W m^{-2} in the heat flux convergence. Other errors in the heat flux convergence, such as that due to temporal aliasing by the quarterly sampling, are estimated to be less that the reference-level error. A conservative estimate for the rms error of the interannual heat flux convergence is 10 W m^{-2}.

b. Heat storage

The rate of heat storage in the Tasman Box control volume is

$$\text{Storage} = \int_{\text{box}} \int_{\bar{z}_{12}}^{0} \rho c_p \frac{\partial T}{\partial t}\, dz\, dA. \quad (7)$$

The error in 1-yr storage estimates is about 5 W m^{-2} (Willis et al. 2003), less than for the heat flux convergence. Heat storage is the simplest part of the heat balance to measure, requiring only temperature profiles, in this case supplemented by AH data. Errors are relatively straightforward to assess, and they decrease with increasing time and space scales, and with data density. The values of storage (Fig. 7, thick blue line) range from about −10 W m^{-2} in 1994 to 26 W m^{-2} at the end of 1997. Variability in storage is related to the depth of the thermocline as well as to the temperature of the surface layer.

c. Air–sea flux

Interannual variability in air–sea flux, from ECMWF operational analysis and averaged over the area of the box, is shown as the thick green line in Fig. 7. Its interannual variability is marginally less than the other two components, but is still about 20 W m^{-2}. The NCEP–NCAR reanalysis (not shown) is similar but with less interannual variability than ECMWF values, and it does not close the time-varying heat balance as well as ECMWF. The accuracy of air–sea flux analyses is not known, and the errors may be larger than in either of the other heat budget components. The mean difference between ECMWF and NCEP–NCAR values averaged over the Tasman Box is 10.5 W m^{-2}, and the standard deviation of interannual differences averaged over the box is 8.0 W m^{-2}, suggesting a lower bound on air–sea flux errors.

d. The balance

How well does the Tasman Box heat budget close? In Fig. 7, each of the thin lines shows one of the heat

budget components calculated as the residual of the other two, that is, heat storage calculated as heat flux convergence less the heat lost due to air–sea flux, and similarly for the other two components. The heat budget closes well in the period 1993–98 (rms imbalance of only 5.5 W m^{-2}), and poorly in 1999–2001. For the 10-yr record with AH data, the mean imbalance as noted in section 3 was 12.3 W m^{-2} using ECMWF air–sea fluxes, and the overall standard deviation was 11.0 W m^{-2}. With NCEP–NCAR reanalysis values, the mean imbalance was 1.8 W m^{-2} and the standard deviation was 11.5 W m^{-2}.

As anticipated, all three components of the heat budget are important on interannual time scales. Ocean circulation always heats the interior of the box, but the range of interannual variability in ocean heat flux convergence (40 W m^{-2}) is as large as its mean value. Heat storage has an equally large range of variability and a small mean value of 1.3 W m^{-2} over 10 yr. Air–sea flux always cools the ocean on interannual time scales, and its variability may be less than the other components. The interannual values of ocean heat flux convergence and air–sea flux are correlated ($r = -0.71$, significant at 95% confidence assuming 10 degrees of freedom), with maxima in the heating of the box by ocean circulation corresponding to maxima in cooling of the box by air–sea flux.

The heat budget has closed reasonably well in that differences between the direct and residual calculations in Fig. 7 (about 10 W m^{-2}) are less than the interannual signals. Certainly one would like to do better, and the prospects for this are discussed in the next section, but the level of agreement in Fig. 7 supports the a priori error estimates for heat flux convergence and storage.

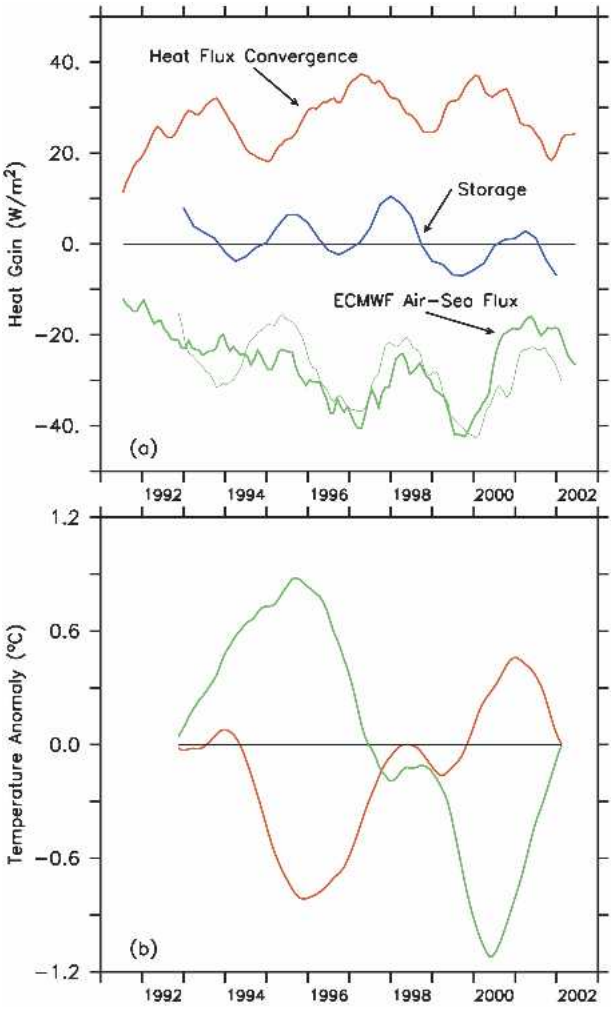

FIG. 8. (a) Heat budget components, as in Fig. 7 except for the upper 100 m only. (b) Time integral of upper 100-m ocean heat flux convergence (red) and air–sea flux (green), expressed as temperature change.

7. Summary and discussion

a. Roles of atmosphere and ocean in the heat budget

Having made progress in closing the oceanic heat budget, the problem of understanding the ocean's role in climate variability of the Tasman region, including New Zealand, is of great interest. The Tasman Box heat budget in Fig. 7 is for all waters warmer than 12°C, an isotherm found as deep as 500 m in the northwest corner of the box (Fig. 1). Hence it includes surface waters subject to air–sea interaction and thermocline waters that are insulated from the atmosphere on interannual time scales. The heat budget is modified in Fig. 8a for a surface-layer control volume, whose bottom boundary is a depth of 100 m. This calculation uses the same horizontal velocity field as the deeper (Fig. 7) calculation, but it is integrated only down to 100-m depth. As an approximation, the divergence of the horizontal transport (geostrophic plus Ekman) above 100 m is assumed to flow vertically across the 100-m surface at the time-varying spatial mean temperature at that depth. The choice of 100 m as the lower integration limit occasionally does not encompass the entire mixed layer, primarily in winter months in the southern portion of the box. In this calculation the heat balance closure is slightly improved (increased ratio of signal variance to residual variance)—with the rms residual having decreased from 11.0 W m^{-2} in Fig. 7 to 6.0 W m^{-2} in Fig. 8a. The interannual heat flux convergence and heat storage terms in Fig. 8a are reduced to about two-thirds of their values in the deeper calculation, and all three terms in the upper 100-m balance have about the same magnitude of variability. The difference between Figs. 7

and 8a reflects the balance of heat storage and heat flux convergence below 100 m.

The cumulative effects of ocean heat flux convergence and air–sea flux on the average temperature in the upper 100 m of the box are shown, separately, in Fig. 8b. These are the time integrals of the respective heat budget terms in Fig. 8a, after removing the time means. The tendency of air–sea flux and ocean heat flux convergence to offset one another is clear in both panels of Fig. 8. The net warming or cooling of the upper 100 m occurs when the forcing terms are not exactly out of phase or have peaks of different amplitude.

On interannual time scales, national mean air temperatures in New Zealand are highly correlated with regional SSTs (Basher and Thompson 1996). Moreover, a correlation between SST and meridional wind on interannual time scales led Basher and Thompson (1996) to conclude that the meridional atmospheric circulation is the primary influence on SST and air temperature. The lag of SST by 1–2 months suggested a mechanism wherein southerly winds directly cool the air, and also, with a small lag, the sea.

Our results (Fig. 8) point to a more complicated mechanism for interannual SST variability in the Tasman Box, and hence atmospheric temperature variability in New Zealand. Analysis of ECMWF air–sea fluxes shows that the interannual variability in the Tasman Box (Fig. 8a, green line) is primarily due to incoming shortwave radiation (i.e., cloudiness), with smaller contributions from latent and sensible heat fluxes and outgoing longwave radiation. The periods of increased cloudiness tend to coincide with increased wind stress curl (shown in Fig. 6 as Ekman convergence), which causes the gyre to spin up through Sverdrup dynamics. A stronger gyre results in greater heat transport southward in the EAC, and a tendency to warm the box. Hence, the atmospheric variability has both a direct effect of diminished incoming radiation and an opposing indirect one of increased ocean heat flux convergence. Changes in surface-layer temperature occur when one or the other of the opposing effects is stronger or the relative phase between them varies. The spinup of the gyre may lag the air–sea flux forcing if the variability in wind stress curl occurs at some distance away from the western boundary. Our time series is not sufficiently long for statistical confidence in this phase difference, but to the eye the larger anomalies in air–sea flux do occur a little earlier than the opposing maxima in heat flux convergence. The tendency of the oceanic response to redden white-noise forcing by the atmosphere may lead to the appearance of a regular periodicity of 2–3 yr in the ocean heat flux convergence

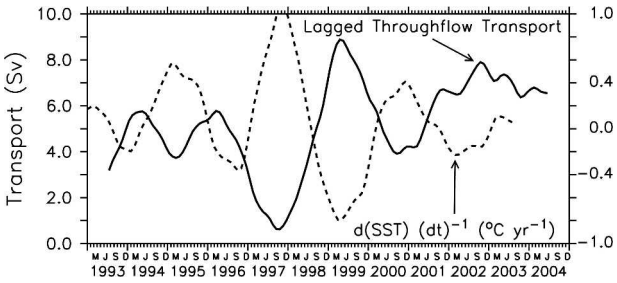

FIG. 9. Throughflow transport (as in Fig. 6 except shifted later in time by 24 months) compared to the time derivative of SST (right-hand scale) averaged over the area of the box.

and heat storage terms. Correlation analysis of SST and atmospheric variability alone suggest a misleadingly simple interpretation of SST evolution, and one must keep in mind that the atmospheric and oceanic variables have similar periodicities and are coupled. The complete picture involves the atmospheric variability affecting SST directly through air–sea fluxes and indirectly through forcing of ocean heat flux convergence.

To illustrate further, and for the sake of argument, another correlation is shown in Fig. 9. The time series of throughflow transport (Fig. 6), shifted later in time by 24 months, is well correlated (-0.75) with the rate of change of SST. This is the strongest correlation we see with SST variability, but it has no simple physical interpretation. While partly a statistical anomaly, it is also symptomatic of the complex relationships inherent in the combined atmospheric and oceanic influences on SST in the region. In such a system, simple correlation analysis does not accurately portray cause and effect. While Fig. 9 suggests significant predictability of regional SST (and hence air temperature) from ocean transport, the understanding of this signal will require an expanded regional study and is beyond the scope of the present work.

Studies of western boundary current heat budgets have also been carried out in the North Pacific (Qiu 2000; Vivier et al. 2002; Kelly 2004) and North Atlantic (Dong and Kelly 2004), and are summarized by Kelly and Dong (2004). These studies used simple models or statistical relationships to estimate the oceanic heat flux convergence, as compared to the calculations from subsurface data in the present work. As in the present analysis and the preliminary Tasman Box calculation by Sprintall et al. (1995), Kelly and Dong (2004) note that interannual variability in ocean heat flux convergence in these western boundary current regions is a large contributor to anomalies in heat content. Moreover, oceanic feedback appears to be significant in the Kuroshio region, with heat content anomalies producing some skill in prediction of air–sea fluxes (Kelly 2004).

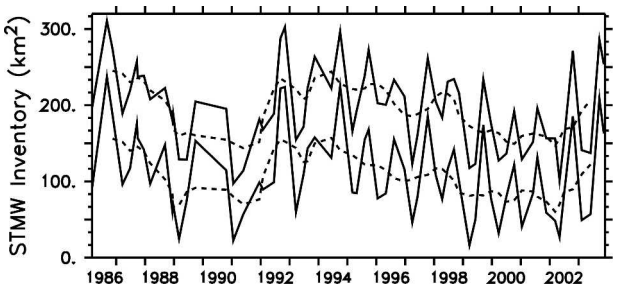

FIG. 10. Time series of STMW inventory north of New Zealand along the PX06 transect (solid lines). The inventory for a given transect is expressed as the cross-sectional area of waters between 14° and 20°C having vertical temperature gradient less than 2.0°C (100 m)$^{-1}$ (upper lines) or 1.6°C (100 m)$^{-1}$ (lower lines). Values are shown for each transect and for the four-cruise running mean (dashed lines). This plot updates Roemmich and Cornuelle's (1992) Fig. 5.

The Tasman Box study is not of long enough duration for a statistical analysis of the relationship between the heat budget components. However, on the longest time scale represented in Fig. 8 (10 yr, one realization), a feedback hypothesis in not inconsistent. The maximum in heat content occurred about 1998, coincident with the largest heat loss to the atmosphere in 1997 and 1999 (Fig. 8a).

b. Subtropical mode water

Along the Auckland–Suva, Fiji (PX06) track, HRX sampling began in 1986, providing a long record of thermal variability. Roemmich and Cornuelle (1992) discussed the variability of STMW along that track, and their plot of STMW variability was updated by Sprintall et al. (1995). Figure 10 shows the newly updated census of STMW volume along PX06. Since there are only four cruises per year and considerable variability, the year-to-year changes are often not significant. However, multiyear trends are reliably depicted. In general, large volumes of STMW occur when the upper-ocean heat content is low (weak stratification, cool surface layer), and small volumes occur when the heat content is high (strong stratification, warm surface layer). Following the sharp increase in STMW volume around 1992, discussed by Sprintall et al. (1995), a long period of decreasing STMW volume accompanied the upper-ocean warming of the mid-1990s. There may be a return to increasing volume in the most recent years, 2002–03. The STMW census along line PX06 reflects the waters leaving the Tasman Box toward the east.

Consistent with the previous section, the variability in STMW volume is due to the residual of heat flux convergence and air–sea flux rather than being dominated by either one. The STMW volume increases during periods when heat loss to the atmosphere exceeds heat gain due to oceanic advection. The preliminary conclusion by Sprintall et al. (1995) that heat flux convergence plays a significant role in regional upper-ocean anomalies is borne out in the decadal dataset.

c. Planned improvements in the observations

While the present results are encouraging, substantial problems are still evident, for example, in the heat budget imbalances exceeding 30 W m^{-2} in 2000 (Fig. 7). The large imbalances are likely due to systematic errors in air–sea fluxes and to errors resulting from the 800-m reference level used in geostrophic calculations. It is necessary to do better, and fortunately there are good prospects for improving all components of the heat budget:

1) There is now a complete suite of high quality surface meteorological instruments [Volunteer Observing System-Improved Meteorology (VOS-IMET)] installed on the (M/V) *Columbus Florida*, which sails along PX06 and through the Tasman Box interior (Auckland–Sydney) on a regular basis. An objective for these instruments is to identify large-scale biases in air–sea flux products.
2) We are presently testing a research-quality deep (2000 m) XBT, with a calibrated thermistor and single-point fall-rate calibration. If successful, this instrument will provide the deeper reference level that is clearly needed in the western boundary current systems.
3) The Argo float project, on completion, will maintain about 30 floats in the Tasman Box operating at 10-day cycles. These will thus provide about 1000 temperature/salinity profiles and 1000-m reference velocities per year. The heat and salt storage terms, as well as the interannual variations in reference velocity on broad spatial scales will be accurately measured.

d. Data analysis and data assimilation modeling

The difficulty of interpreting the heat budget and its components illustrates the need for dynamically consistent models that can utilize the increasingly sophisticated ocean datasets now being collected and can be used to understand the complex coupled behavior of the climate system. Just as the datasets are being improved, so are the interpretive modeling tools. An analysis of global and regional ocean heat budgets was carried out by Stammer et al. (2003) using an ocean general circulation model constrained by global datasets. There is still much work to be done to ensure that such models adequately represent the physics of

ocean circulation and the growing datasets used to constrain the models.

Acknowledgments. HRX lines PX06, PX30, and PX34 are carried out on a collaborative basis by Scripps Institution of Oceanography (United States), CSIRO Marine Research (Australia), and the National Institute of Water and Atmospheric Research (New Zealand). For the U.S. component, collection of the XBT/XCTD data is supported by the National Science Foundation through Grant OCE00-95248. Analysis was supported by the NASA JASON-1 project through JPL Contract 961424 and by NOAA Grant NA17RJ1231. Valuable comments on the manuscript were provided by K. Kelly and an anonymous reviewer. We are grateful for the dedicated efforts of many ship riders in collecting the XBT/XCTD data. We especially thank the captains, officers, and crew of the numerous ships assisting in the collection of the HRX data. The National Center for Atmospheric Research provided access to ECMWF analysis products. Graphics were produced using FERRET, developed by NOAA/PMEL.

REFERENCES

Basher, R., and C. Thompson, 1996: Relationship of air temperatures in New Zealand to regional anomalies in sea-surface temperature and atmospheric circulation. *Int. J. Climatol.,* **16,** 405–425.

Davis, R., 1998: Preliminary results from directly measured mid-depth circulation in the tropical and South Pacific. *J. Geophys. Res.,* **103,** 24 619–24 639.

Dong, S., and K. A. Kelly, 2004: The heat budget in the Gulf Stream region: The importance of heat storage and advection. *J. Phys. Oceanogr.,* **34,** 1214–1231.

Ducet, N., P.-Y. Le Traon, and G. Reverdin, 2000: Global high resolution mapping of ocean circulation from TOPEX/Poseidon and ERS-1 and -2. *J. Geophys. Res.,* **105,** 19 477–19 498.

ECMWF, 1993: The description of the ECMWF WCRP III: A global atmospheric data archive. Tech. Attachment 1-18, Reading, United Kingdom, 72 pp.

Gilson, J., D. Roemmich, B. Cornuelle, and L.-L. Fu, 1998: Relationship of TOPEX/Poseidon altimetric height to steric height and circulation in the North Pacific. *J. Geophys. Res.,* **103,** 27 947–27 965.

Kalnay, E., and Coauthors, 1996: The NCEP/NCAR 40-Year Reanalysis Project. *Bull. Amer. Meteor. Soc.,* **77,** 437–471.

Kelly, K., 2004: The relationship between oceanic heat transport and surface fluxes in the western North Pacific: 1970–2000. *J. Climate,* **17,** 573–588.

——, and S. Dong, 2004: The relationship of western boundary current heat transport and storage to midlatitude ocean–atmosphere interaction. *Earth's Climate: The Ocean–Atmosphere Interaction, Geophys. Monogr.*, No. 147, Amer. Geophys. Union, 347–364.

Morris, M., D. Roemmich, and B. Cornuelle, 1996: Observations of variability in the South Pacific subtropical gyre. *J. Phys. Oceanogr.,* **26,** 2359–2380.

Qiu, B., 2000: Interannual variability of the Kuroshio Extension system and its impact on the wintertime SST field. *J. Phys. Oceanogr.,* **30,** 1486–1502.

Reid, J., 1986: On the total geostrophic circulation of the South Pacific Ocean: Flow patterns, tracers, and transports. *Progress in Oceanography,* Vol. 16, Pergamon, 1–62.

Ridgway, K. R., and J. S. Godfrey, 1994: Mass and heat budgets in the East Australian Current—A direct approach. *J. Geophys. Res.,* **99,** 3231–3248.

——, and J. R. Dunn, 2003: Mesoscale structure of the mean East Australian Current System and its relationship to topography. *Progress in Oceanography,* Vol. 56, Pergamon, 189–222.

Roemmich, D. H., and B. Cornuelle, 1990: Observing the fluctuations of gyre-scale ocean circulation: A study of the subtropical South Pacific. *J. Phys. Oceanogr.,* **20,** 1919–1934.

——, and ——, 1992: The subtropical mode waters of the South Pacific Ocean. *J. Phys. Oceanogr.,* **22,** 1178–1187.

Sprintall, J., D. Roemmich, B. Stanton, and R. Bailey, 1995: Regional climate variability and ocean heat transport in the southwest Pacific Ocean. *J. Geophys. Res.,* **100,** 15 865–15 871.

Stammer, D., and Coauthors, 2003: Volume, heat, and freshwater transports of the global ocean circulation 1993–2000, estimated from a general circulation model constrained by World Ocean Circulation Experiment (WOCE) data. *J. Geophys. Res.,* **108,** 3007, doi:10.1029/2001JC001115.

Stanton, B., and P. Sutton, 2003: Velocity measurements in the East Auckland Current north-east of North Cape, New Zealand. *N. Z. J. Mar. Freshwater Res.,* **37,** 195–204.

——, ——, and S. Chiswell, 1997: The East Auckland Current, 1994–95. *N. Z. J. Mar. Freshwater Res.,* **31,** 537–549.

Vivier, F., K. Kelly, and L. Thompson, 2002: Heat budget in the Kuroshio Extension region: 1993–99. *J. Phys. Oceanogr.,* **32,** 3436–3454.

Wijffels, S., E. Firing, and H. Bryden, 1994: Direct observations of the Ekman balance at 10°N in the Pacific. *J. Phys. Oceanogr.,* **24,** 1666–1679.

Willis, J. K., D. Roemmich, and B. Cornuelle, 2003: Combining altimetric height with broadscale profile data to estimate steric height, heat storage, subsurface temperature, and sea-surface temperature variability. *J. Geophys. Res.,* **108,** 3292, doi:10.1029/2002JC001755.